Table 1 Summary of intraoperative and final findings

Case	Age/sex	Frozen HE	MIB-1 (R-IHC)	Frozen HE + R-IHC	Permanent MIB-1	Final diagnosis
a. Hokkaido University						
1[a]	48/F	II	3.5	II	3	II
2[a]	37/M	II	2.7	II	4.5	II
3	62/M	II	3.2	II	4	II
4	37/F	II or gliosis	2.1	II	2.6	II
5	16/M	II	0.5	II	0.1	II
6	37/M	II or III	6.7	II	5	II
7	63/F	III	5	III	6	III
8	55/F	IV	15.1	IV	15	IV
9	83/M	IV	16.7	IV	30	IV
10	60/F	IV	15.6	IV	39.7	IV
11	59/M	III or IV	20.4	III or IV	25	IV
12	39/M	IV	12	IV	25	IV
13	30/F	II or III	23	III	15	III
14	81/F	IV	28	IV	50	IV
15	65/M	IV	25.8	IV	50	IV
b. Akita University						
16	4/F	I	0.5	I	2	I
17	32/F	II	2	I	8	II
18	43/F	II	0.2	I	1.8	II
19	49/M	II or III	0.1	II	2.7	II
20	29/M	II or III	15	III	17.9	III
21	32/F	II	4	II	12.7	III
22	33/M	II or III	20	III	25.6	III
23	46/F	III or IV	15	III or IV	23	IV
24	50/F	IV	25	IV	36.7	IV
25	60/M	IV	30	IV	28.9	IV
26	63/M	IV	12	IV	14.3	IV
27	65/M	IV	39.5	IV	77.4	IV
28	69/F	IV	26.7	IV	40.4	IV
29	71/F	IV	25	IV	40	IV
30	72/M	IV	30	IV	26.7	IV
31	74/F	III or IV	46	IV	81	IV
32	76/F	IV	10	IV	11.7	IV
33	87/M	IV	66	IV	71	IV

[a] Recut section from reserved frozen blocks

facilitate the reaction. R-IHC for Ki-67/MIB-1, CD3, and CD20 was performed using frozen sections used for intraoperative diagnosis.

Standard IHC for permanent tissues

Standard IHC was performed as described elsewhere [15]. Briefly, sectioned specimens were incubated with primary antibody at RT for 60 min and washed with PBS with 0.05 % Tween20 for 5 min 3 times, and then incubated with Envision at RT for 30 min. Reacted antibodies were visualized by enzyme reaction with DAB as a substrate. Standard IHC for Ki-67/MIB-1, CD3, and CD20 was performed using FFPE sections used for permanent diagnosis.

Antibodies

The following antibodies were used as the primary antibody with the appropriate dilution shown in parentheses: monoclonal mouse anti-Ki-67/MIB-1 antibody (monoclonal, clone MIB-1; Dako, 1:100), anti-CD20 antibody

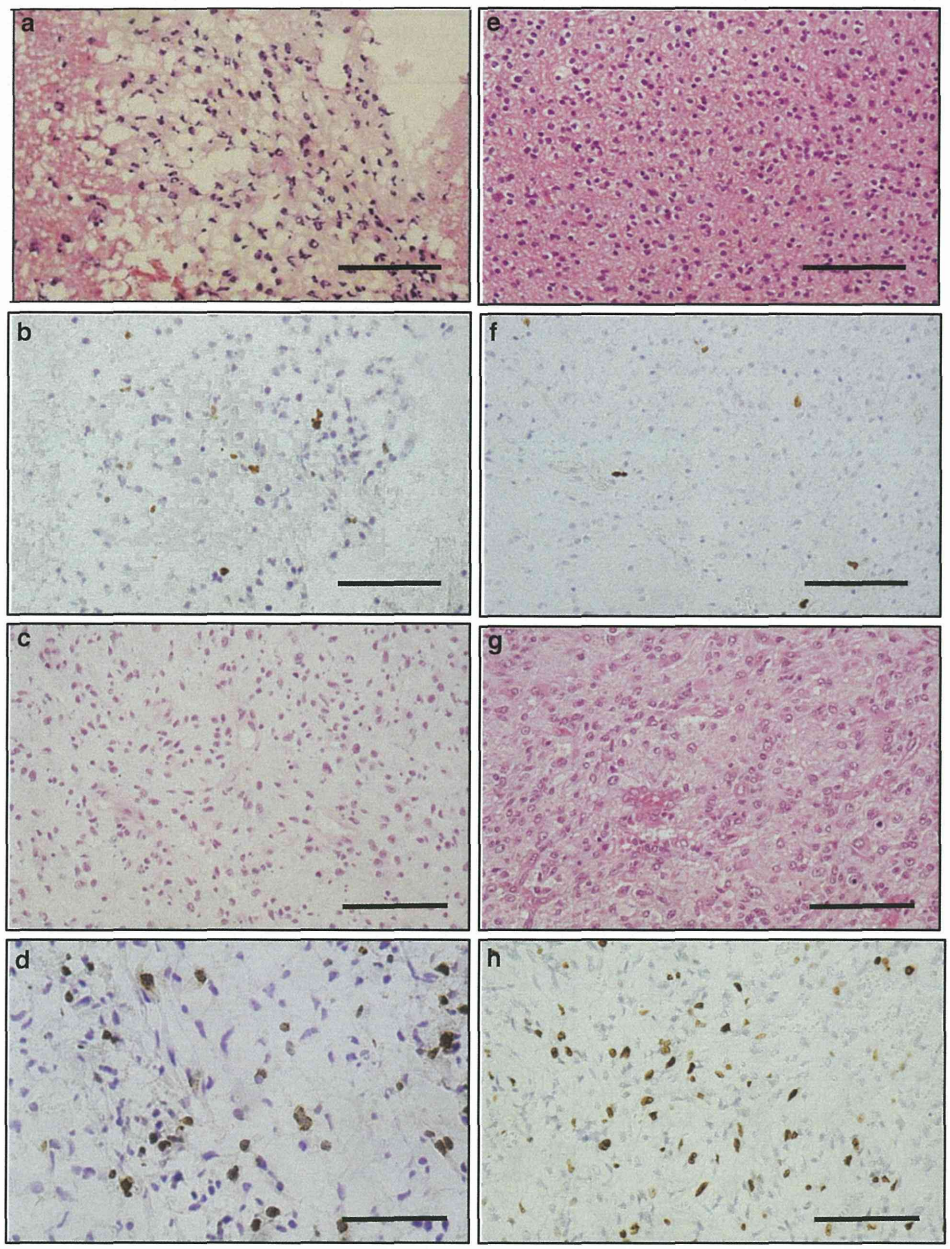

Fig. 1 Histological findings in Case 6 (**a** H&E staining in frozen specimen, **b** Ki-67/MIB-1 staining by R-IHC in frozen specimen, **c** H&E staining in FFPE specimen, **d** Ki-67/MIB-1 staining by standard IHC in FFPE specimens). Histological findings in Case 13 (**e** H&E staining in frozen specimen, **f** Ki-67/MIB-1 staining by R-IHC in frozen specimen, **g** H&E staining in FFPE specimen, **h** Ki-67/MIB-1 staining by standard IHC in FFPE specimen). *Scale bars* 20 μm

(monoclonal, clone L26; Dako, 1:400), and anti-CD3 antibody (polyclonal, rabbit; Dako, 1:200).

Statistical analysis

The correlation between frozen and permanent sections of Ki-67/MIB-1 indices was evaluated by Pearson's correlation coefficient. A value of $P < 0.05$ was considered as significant.

Results

Limitation of the accuracy of intraoperative diagnosis of CNS tumors without R-IHC

The overall diagnostic accuracy (the complete correlation) was 90.7 % (168/183 cases), and this was as high as the accuracy described in previous studies. The accuracy for each diagnosis was as follows: glioma 91 % (94/103),

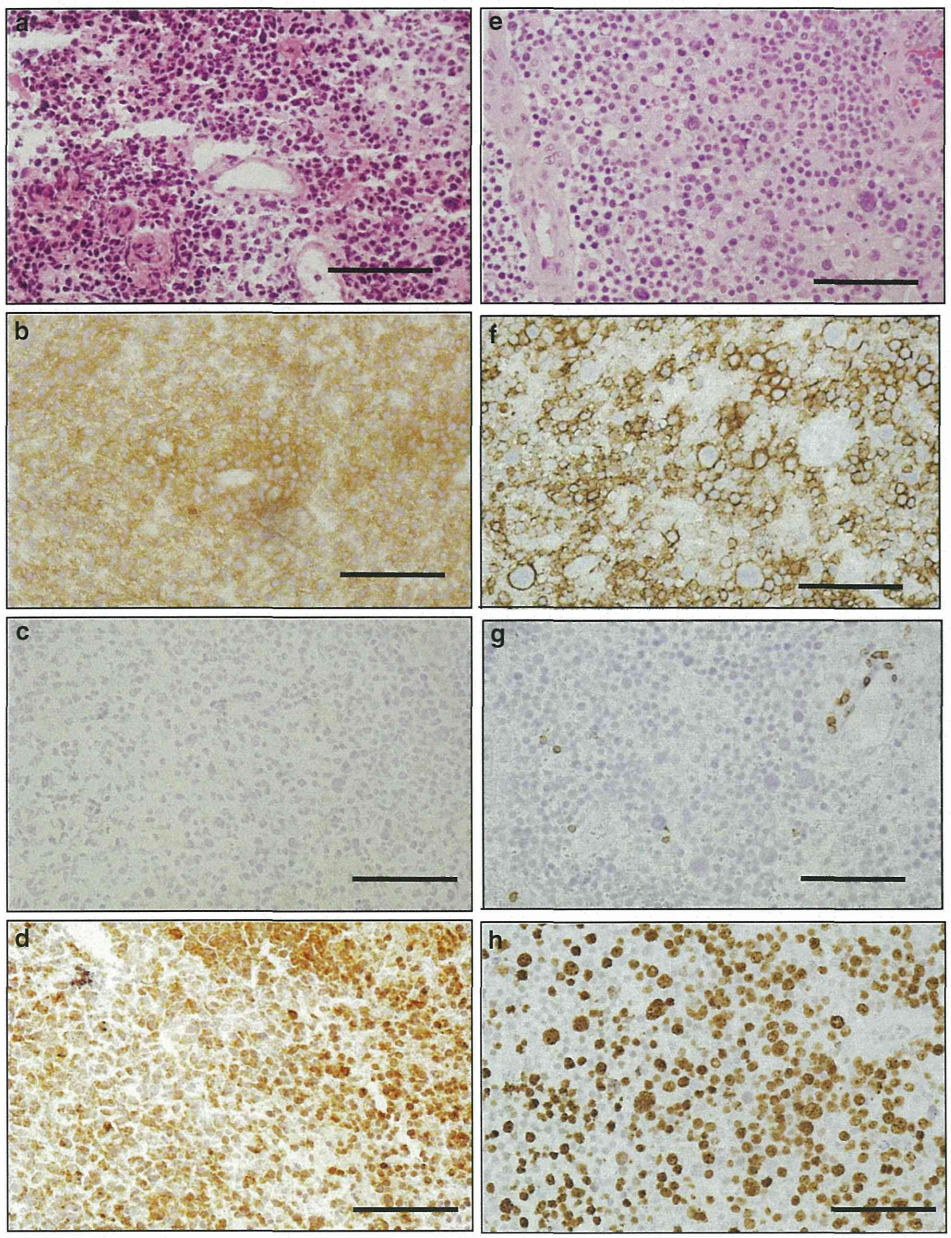

Fig. 2 Histological findings of frozen specimen in Case 37 (**a** H&E staining, **b** CD20 staining by R-IHC, **c** CD3 staining by R-IHC, **d** Ki-67/MIB-1 staining by R-IHC), and FFPE specimens for final diagnosis (**e** H&E staining, **f** CD20 staining by standard IHC, **g** CD3 staining by standard IHC, **h** Ki-67/MIB-1 staining by standard IHC). *Scale bars* 20 μm

metastatic carcinoma 100 % (34/34), meningioma 90 % (19/21), CNS lymphoma 50 % (4/8), shcwannoma 66 % (4/6), and craniopharyngioma 100 % (2/2). The partial correlation was 8.2 % (15/183 cases) and no correlation was 1.1 % (2/183 cases). In these two no-correlation cases, we could not determine the glioma grading even as low or high grade, and failed to make a differential diagnosis of glioma from lymphoma.

Application of intraoperative R-IHC for Ki-67/MIB-1 to diagnosis of glioma

In case of the discrimination of low- and high-grade glioma, Ki-67/MIB-1 index may become supportive information, and R-IHC can be completed within 16 min and provide clear staining of Ki-67/MIB-1. Both in Case 6 and Case 13, H&E staining for frozen specimens showed increased cell

Table 2 Summary of intraoperative and final findings

Case	Age/ sex	Frozen HE	CD20 (R-IHC)	MIB-1 (R-IHC) (%)	Frozen HE + R-IHC	Permanent MIB-1 (%)	Final Dx.
34	68/F	CNSL	diffuse	90	CNSL	100	CNSL
35[a]	86/F	CNSL	diffuse	90	CNSL	90	CNSL
36[a]	49/F	CNSL	diffuse	50	CNSL	60	CNSL
37[a]	62/F	HGG or CNSL	diffuse	90	CNSL	90	CNSL

[a] Recut section from reserved frozen blocks

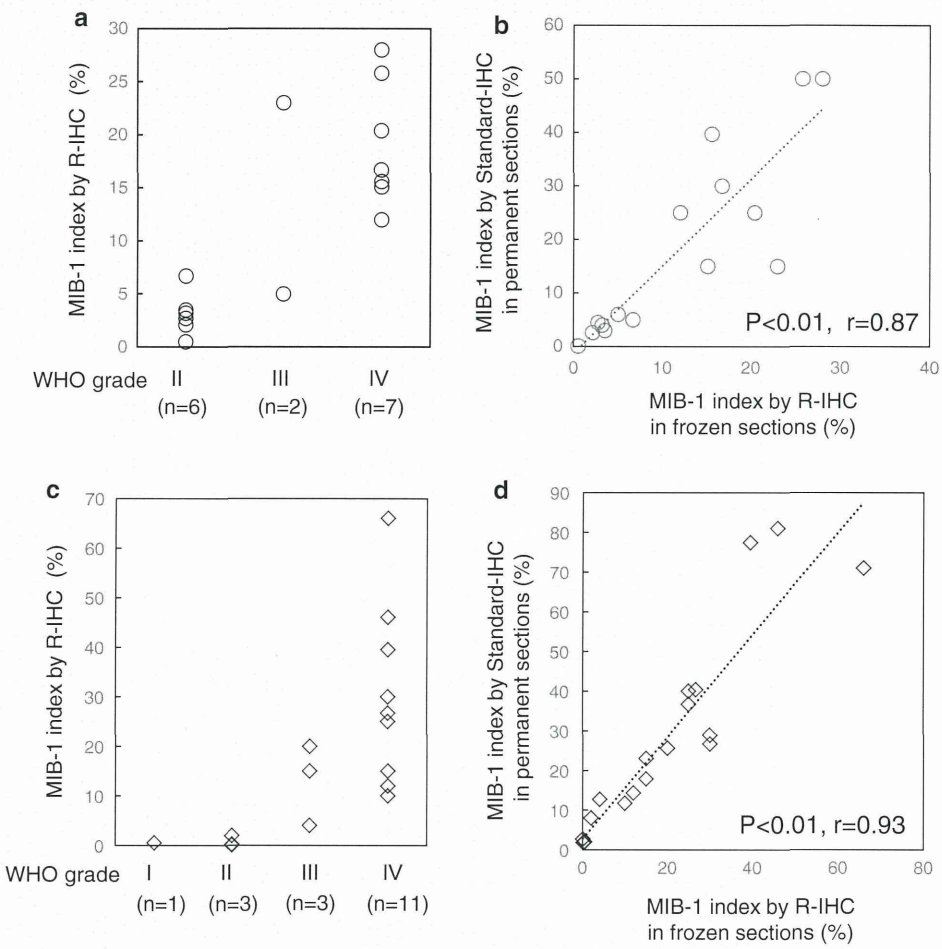

Fig. 3 Ki-67/MIB-1 indices in frozen and FFPE specimens in glioma. **a** Ki-67/MIB-1 indices by R-IHC in 15 frozen specimens of grade II–IV glioma at Hokkaido University. **b** Ki-67/MIB-1 indices by R-IHC in 18 frozen specimens of grade I–IV glioma at Akita University Hospital. **c** Correlation between Ki-67/MIB-1 indices by R-IHC using frozen specimens and those by standard IHC using FFPE specimens at Hokkaido University. **d** Correlation between Ki-67/MIB-1 indices by R-IHC using frozen specimens and those by standard IHC using FFPE specimens at Akita University Hospital

numbers with nuclear atypia suggesting diagnosis as grade II or III glioma (Fig. 1a, c). Using R-IHC, Ki-67/MIB-1 index in frozen specimens was 6.7 and 23 %, respectively (Fig. 1b, d); thus, we considered Case 6 as being grade II and Case 13 as grade III. These decisions were consistent with the final diagnosis using FFPE tissues with Ki-67/MIB-1 index in ordinal IHC (Fig. 1e–h; Table 1a).

Application of intraoperative R-IHC for lymphocyte surface antigen for diagnosis of CNS lymphoma

For the intraoperative diagnosis, discrimination between glioma and lymphoma is occasionally difficult without any support of R-IHC. Thus, we examined the application of lymphocyte surface antigen to R-IHC methods, and among the four cases of CNS lymphoma analyzed, CD20 and Ki-67/MIB-1 indices were successfully stained in all frozen samples using R-IHC. Ki-67/MIB-1 indices were as high as those found in permanent sections (Fig. 2; Table 2).

Comparison of the results of Ki-67/MIB-1 in glioma between R-IHC for frozen tissues and standard IHC for FFPE tissues

Clinicopathological application of the new R-IHC machine to CNS tumor diagnosis was evaluated. The diagnosis of

Table 3 Representative rapid IHC methods

Author	Year	Method	Ki-67 Ab clone	Dilution	Total time (min)	Reference
Ichihara et al.	1989	Microwave	ND	ND	13	[7]
Richiter et al.	1999	EPOS	ND	ND	12	[8]
Kammerer et al.	2001	Modified EnVision	KISS	1:10	12	[9]
Haapasalo et al.	2005	Ultrarapid-ki67 kit	ND	ND	14	[10]
Monig et al.	2006	En Vision, Histofine	ND	ND	10–13	[12]
Hatta et. al.	2006	Intermittent microwave	ND	ND	15	[13]
Hatta et al.	2010	Ultrasound	MIB-1	1:40	10	[14]
Uzuka et al.	2011	Vectastain kit	MIB-1	1:200	70	[11]
Toda et al.	2011	AC field	ND	ND	21	[15]
Tanino et al.	2014	AC field	MIB-1	1:100	16	This study

ND not determined

H&E stain with or without Ki-67/MIB-1 index in frozen sections and final diagnosis with immunohistochemistry in permanent sections of this study were shown in Table 1a, b. As measurement of Ki-67/MIB-1 index is critical for glioma grading, we compared the results of immunostaining of Ki-67/MIB-1 between R-IHC for frozen tissues and standard IHC for FFPE tissues in two independent facilities, Hokkaido University and Akita University.

Correlation of Ki-67/MIB-1 indices with glioma grading was observed with grade II as 2.4 ± 1.2 (SD) %, grade III as 11.6 ± 9.9 (SD) %, and grade IV as 19.1 ± 5.9 (SD) % in Hokkaido University and grade I as 0.5 %, grade II as 0.8 ± 1.1 (SD) %, grade III as 13.0 ± 8.2 (SD) %, and grade IV as 29.6 ± 16.3 (SD) % in Akita University (Fig. 3a, b). In addition, the Ki-67/MIB-1 indices based on R-IHC for frozen sections significantly correlated with those of permanent sections in both Hokkaido University ($P < 0.01$, $r = 0.87$) and Akita University ($P < 0.01$, $r = 0.93$) (Fig. 3c, d).

Discussion

We have established a new machine for R-IHC based on a novel principle of AC-facilitated antigen–antibody reaction, by which the turnaround time to obtain the results for surgeons in case of intraoperative diagnosis can be almost within 30 min. It is obvious that this new R-IHC method can be applied for various specimens of the intraoperative diagnosis, but it should also possess advantages in the field of CNS tumor diagnosis. To ensure the requirement of R-IHC for the intraoperative diagnosis of CNS tumors, we have surveyed our 183 cases and found that the accuracy of the intraoperative diagnostic without IHC was 90.7 %, as same as in previous reports. Among them, the most difficult diagnosis was glioma grading, especially discrimination between grade II and grade III. In this study, we clarified that R-IHC for Ki-67/MIB-1 index can provide important information for glioma grading in two independent institutes. Ki-67/MIB-1 indices of R-IHC in frozen sections were statistically correlated to those of conventional IHC in permanent sections. In addition, discrimination of CNS lymphoma from glioma was occasionally difficult, and this new R-IHC method clearly demonstrated the positivity of the lymphocyte surface antigen CD20. Although R-IHC obviously provides further information about the tumor, the number of analyzed cases in this study was not enough to provide clear cut-off value for Ki-67/MIB-1 index according to the WHO grading. Furthermore, we should notice that the limitation of intraoperative diagnosis using R-IHC was mainly due to sampling divergency including tumor heterogeneity in glioma, poor demarcation of CNS lymphoma, and differential location of sampling. Indeed, Ki-67/MIB-1 index by R-IHC in Case 21 was not matched with that by standard IHC by the tumor heterogeneity.

Similar to our present study, several groups have reported the limitations of intraoperative diagnosis of CNS tumors such as glioma grading and determination of astrocytic versus oligodendroglial origin in addition to the differential diagnosis of CNS lymphoma, spindle cell lesions, reactive lesions as gliosis, poorly differentiated metastatic carcinoma, and primitive neuroectodermal tumor (PNET) [5, 11]. In this study, as we focused on the utility for diagnosis of glioma and CNS lymphoma using limited number of antibodies as Ki-67/MIB-1, CD3 and CD20, we could not distinguish between astrocytic and oligodendroglial tumors. The combination of several markers will provide more precise diagnosis in the future. At least, to distinguish gliosis from low-grade glioma, Ki-67/MIB-1 by R-IHC is useful as shown in Case 4. In the near future, application of anti-IDH1-R132H antibody on this R-IHC method is expected to the discrimination of glioma and gliosis.

To date, several methods for R-IHC were proposed including microwave, specific reagent, and a combination of microwave and ultrasound, but such specific methods have not been widely accepted in the field of clinicopathological diagnosis for several reasons, such as the requirement of higher concentrated primary antibody or non-specific reaction due to the possible increase of temperature of the specimens by microwave. By our new method, fine staining can be obtained using standard or sometimes lower concentrations of primary antibodies compared to standard IHC methods (data not shown). As compared to another R-IHC methods for Ki-67/MIB-1, our method would be more beneficial from the standpoint of antibody concentration (Table 3). In addition, we have measured the temperature of the specimens within AC stimulation and found a constant temperature (data not shown).

In conclusion, the new R-IHC method using AC field provides reliable results of IHC for CNS tumor diagnosis on frozen sections, and will contribute to an appropriate intraoperative rapid diagnosis.

Acknowledgments This work was supported in part by the Japan Society for the Promotion of Science (JSPS) Grant-in-Aid for Scientific Research (KAKENHI Grant Number 24590406) to M.T. and (KAKENHI Grant Number 23390311) to Y.M.

Appendix: R-IHC Study Group

Shinya Tanaka, Mishie Tanino, Tomoko Takenami, Shiori Akesaka, Manami Watanabe, Eiko Aoyanagi (Hokkaido University), Akira Kurose, Emiko Mizuki, Naoya Kumagai (Hirosaki University), Yu Sugai, Noriyuki Yamada, Chikako Tomizawa (Iwate Medical University), Mareyuki Endo, Miki Aoki, Akira Morohashi, Tomoko Konta (Sendai Kousei Hospital), Kiyotaka Onodera, Manabu Suzuki, Yoshiki Kogi, Satoshi Ota, Yukio Nakatani (Chiba University), Takeo Yano, Tokuyoshi Maruyama, Tomohide Ogura, Jyunya Takeyama, Kazuki Kaneyama, Yoshiyuki Omura, Taizo Shiraishi (Mie University), Tomoo Ito, Yasuhiro Sakai, Emii Yanagida, Naoko Imagawa, Hiroshi Yamada, Tatsuko Tsukamoto (Kobe University), Shiro Takegami (Tohoku University), Satoru Kamata, Eichi Suzuki, Yoichi Akagami, Masami Kagaya, Ryuta Nakamura (Akita Industrial Technology Center), Shunsuke Wakayama, Yoshihiro Minamiya, Toshio Sasajima, Akiteru Goto, Hiroshi Nanjyo, Satoshi Ito, Hayato Konno, Yashushi Kawaharada, Shinnosuke Watanabe, Tomoaki,Yoshioka, Kasumi Narita, Naoko Takahashi, Satoshi Kudou (Akita University).

References

1. Brat DJ, Prayson RA, Ryken TC et al (2008) Diagnosis of malignant glioma: role of neuropathology. J Neurooncol 89(3):287–311
2. Faehndrich J, Weidauer S, Pilatus U et al (2011) Neuroradiological viewpoint on the diagnostics of space-occupying brain lesions. Clin Neuroradiol 21(3):123–139
3. Nihashi T, Dahabreh IJ, Terasawa T (2013) Diagnostic accuracy of PET for recurrent glioma diagnosis: a meta-analysis. AJNR 34(5):944–950 S1–S11
4. Louis DN, Ohgaki H, Wiestler OD et al (2007) WHO classification of tumors of the central nervous system. IARC, Lyon
5. Plesec TP, Prayson RA (2007) Frozen section discrepancy in the evaluation of central nervous system tumors. Arch Pathol Lab Med 131(10):1532–1540
6. Uematsu Y, Owai Y, Okita R et al (2007) The usefulness and problem of intraoperative rapid diagnosis in surgical neuropathology. Brain Tumor Pathol 24(2):47–52
7. Ichihara T, Nakao A, Suzuki Y et al (1989) Improvement of the rapid immunoperoxidase staining method for intraoperative pathological diagnosis of pancreatic cancer using microwave irradiation. J Surg Oncol 42(3):209–214
8. Richter T, Nahrig J, Komminoth P et al (1999) Protocol for ultrarapid immunostaining of frozen sections. J Clin Pathol 52(6):461–463
9. Kammerer U, Kapp M, Gassel AM et al (2001) A new rapid immunohistochemical staining technique using the EnVision antibody complex. J Histochem Cytochem 49(5):623–630
10. Haapasalo J, Mennander A, Helen P et al (2005) Ultrarapid Ki-67 immunostaining in frozen section interpretation of gliomas. J Clin Pathol 58(3):263–268
11. Uzuka T, Aoki H, Natsumeda M et al (2011) Indication of intraoperative immunohistochemistry for accurate pathological diagnosis of brain tumors. Brain Tumor Pathol 28(3):239–246
12. Monig SP, Luebke T, Soheili A et al (2006) Rapid immunohistochemical detection of tumor cells in gastric carcinoma. Oncol Rep 16(5):1143–1147
13. Hatta H, Tsuneyama K, Kumada T et al (2006) Freshly prepared immune complexes with intermittent microwave irradiation result in rapid and high-quality immunostaining. Pathol Res Pract 202(6):439–445
14. Hatta H, Tsuneyama K, Kondo T et al (2010) Development of an ultrasound-emitting device for performing rapid immunostaining procedures. J Histochem Cytochem 58(5):421–428
15. Toda H, Minamiya Y, Kagaya M et al (2011) A novel immunohistochemical staining method allows ultrarapid detection of lymph node micrometastases while conserving antibody. Acta Histochem Cytochem 44(3):133–139
16. Firlik KS, Martinez AJ, Lunsford LD (1999) Use of cytological preparations for the intraoperative diagnosis of stereotactically obtained brain biopsies: a 19-year experience and survey of neuropathologists. J Neurosurg 91(3):454–458

OPEN ACCESS Freely available online

PLOS ONE

Trans-Homophilic Interaction of CADM1 Activates PI3K by Forming a Complex with MAGuK-Family Proteins MPP3 and Dlg

Shigefumi Murakami[◔], **Mika Sakurai-Yageta**[◔], **Tomoko Maruyama, Yoshinori Murakami***

Division of Molecular Pathology, Institute of Medical Science, The University of Tokyo, Tokyo, Japan

Abstract

CADM1 (Cell adhesion molecule 1), a cell adhesion molecule belonging to the immunoglobulin superfamily, is involved in cell-cell interaction and the formation and maintenance of epithelial structure. Expression of CADM1 is frequently down-regulated in various tumors derived from epithelial cells. However, the intracellular signaling pathways activated by CADM1-mediated cell adhesion remain unknown. Here, we established a cell-based spreading assay to analyze the signaling pathway specifically activated by the *trans*-homophilic interaction of CADM1. In the assay, MDCK cells expressing exogenous CADM1 were incubated on the glass coated with a recombinant extracellular fragment of CADM1, and the degree of cell spreading was quantified by measuring their surface area. Assay screening of 104 chemical inhibitors with known functions revealed that LY294002, an inhibitor of phosphoinositide 3-kinase (PI3K), efficiently suppressed cell spreading in a dose-dependent manner. Inhibitors of Akt and Rac1, downstream effectors of PI3K, also partially suppressed cell spreading, while the addition of both inhibitors blocked cell spreading to the same extent as did LY294002. Furthermore, MPP3 and Dlg, membrane-associated guanylate kinase homologs (MAGuK) proteins, connect CADM1 with p85 of PI3K by forming a multi-protein complex at the periphery of cells. These results suggest that *trans*-homophilic interaction mediated by CADM1 activates the PI3K pathway to reorganize the actin cytoskeleton and form epithelial cell structure.

Citation: Murakami S, Sakurai-Yageta M, Maruyama T, Murakami Y (2014) *Trans*-Homophilic Interaction of CADM1 Activates PI3K by Forming a Complex with MAGuK-Family Proteins MPP3 and Dlg. PLoS ONE 9(2): e82894. doi:10.1371/journal.pone.0082894

Editor: Antimo Migliaccio, II Università di Napoli, Italy

Received April 26, 2013; **Accepted** November 7, 2013; **Published** February 4, 2014

Funding: This work was supported by a Grant-in-Aid for Scientific Research (B) [22300336 and 25290051 for Y.M.]; a Grant-in-Aid for Young Scientists (B) [21790309 and 24790310 for M.SY.]; from the Ministry of Education, Culture, Sports, Science, and Technology, Japan; and a Grant-in-Aid for the Third Term Comprehensive Control Research for Cancer from the Ministry of Health, Labor, and Welfare, Japan [22090601 and 23120701 for Y.M.]. The authors also thank the Screening Committee of Anticancer Drugs, supported by a Grant-in-Aid for Scientific Research in the Priority Area "Cancer" from The Ministry of Education, Culture, Sports, Science, and Technology, Japan, for the SCADS inhibitor kit. The funders had no role in study design, data collection and analysis, decision to publish, or preparation of the manuscript.

Competing Interests: The authors declare that no competing interests exist.

* E-mail: ymurakam@ims.u-tokyo.ac.jp

◔ These authors contributed equally to this work.

Introduction

Cell surface proteins are important for recognizing the external environment and transmitting the information to the cytoplasmic regions through intracellular signaling pathways. Cell responses, such as proliferation, differentiation, apoptosis, or migration, are determined by different signaling pathways. Recently, cell adhesion molecules (CAMs)' role in signal transduction has emerged in addition to their classical roles in cell adhesions [1,2]. CAMs interact with growth factor receptors on plasma membranes or adaptor molecules in juxtamembrane regions. For instance, N-cadherin and NCAM interact with FGFR to promote its signaling in neuronal cells [3]. In epithelial cells, E-cadherin recruits β-catenin in its cytoplasmic domain to organize cell adhesion machinery. However, once intracellular adhesion by E-cadherin is abrogated, E-cadherin and β-catenin dissociate from each other, and β-catenin acts as an important effector in the Wnt signaling pathway; free β-catenin accumulates in the cytoplasm, moves into the nucleus, and then stimulates the transactivation of TCF/LEF for cell proliferation [4].

Cell adhesion molecule 1 (CADM1), cell adhesion molecules of the immunoglobulin superfamily (IgCAMs), contains three extracellular Ig-like loops, a single transmembrane domain, and a short intracellular carboxy-terminal tail [5]. CADM1 is also known as TSLC1, Necl-2, IgSF4A, and SynCAM1 [6]. CADM1 is expressed diffusely in the lateral membrane of cell-cell attachment sites in polarized epithelia, whereas, expression of CADM1 is frequently lost or reduced in a variety of advanced-stage human cancers of the lung, prostate, liver, pancreas, and breast [6]. Considering that the disruption of cell-cell adhesion in epithelial cells triggers tumor cell invasion and metastasis, CADM1 is one of the crucial tumor suppressors involved in cell adhesion like E-cadherin. In fact, CADM1 has a cell aggregation activity when introduced into MDCK cells lacking endogenous CADM1 expression. However, the cytoplasmic signaling pathways triggered by *trans*-homophilic interaction of CADM1 have not been fully elucidated.

The cytoplasmic domain of CADM1 in 46 amino acids contains a protein 4.1-binding motif and a class II PSD95/Dlg/ZO-1 (PDZ)-binding motif. We have demonstrated that CADM1 is

connected to the actin cytoskeleton through direct interaction with protein 4.1B [7]. CADM1 also associates with members of a group of scaffolding proteins, membrane-associated guanylate kinase homologs (MAGuKs), including MPP1-3, CASK, and Pals-2, through a class II PDZ-binding motif [8–11]. MAGuKs contain multiple protein-protein interaction modules, including PDZ, SH3, and GuK domains, that allow the clustering of transmembrane proteins and MAGuKs themselves [12]. In neuronal synapses, many MAGuKs, such as PSD-95, SAP102, SAP97/hDlg, and CASK, are localized at pre- and post-synaptic regions and are implicated in synaptic plasticity through the clustering of receptors [13]. In addition, one MAGuK, CARMA1, associates with PKC-θ and Bcl10 and activates NFκ-B signaling in T cells [14]. Thus, MAGuK-family proteins appeared to be important downstream molecules of CAMs, including CADM1, for intracellular signal transduction. However, the precise role of the interaction of CADM1 with MAGuKs remains to be understood.

In the present study, we established a cell-based assay to identify signaling pathways involved in cell spreading mediated by *trans*-homophilic interaction of CADM1. Distinct from a simple cell adhesion, cell spreading is a process that requires cytoplasmic signaling to generate actin reorganization mediated by *trans*-homophilic interaction of CADM1. By treating cells with 104 different chemical inhibitors with known target pathways, we identified that phosphoinositide 3-kinase (PI3K) signaling leading to actin rearrangement was essential for CADM1-mediated cell spreading. We further demonstrated that CADM1 was connected to PI3K by forming a protein complex with MPP3 and Dlg at the cell-cell contact sites.

We propose that CADM1 is implicated in transmitting cell attachment signals to actin reorganization in the cytoplasm through activating the PI3K pathway for the formation and maintenance of adhesion-based epithelial structure.

Materials and Methods

Expression Vectors, Cell Culture, Transfection, Antibodies, Reagents, Immunoprecipitation, Western Blotting, and Cell Aggregation Assay

These are described in detail in the Methods S1.

Purification of Recombinant CADM1-EC-Fc

HEK293 cells stably expressing a secreted form of CADM1-EC-Fc were cultured in GIT medium for 3 days after the cells reached confluence (Wako Pure Chemical Industries, Ltd., Osaka, Japan). Then, the conditioned medium was collected, and CADM1-EC-Fc was purified using the Affi-Gel Protein A MAPS II kit (Bio-Rad) and dialyzed against phosphate-buffered saline (PBS).

Cell Spreading Assay

Coverslips were pre-coated with 50 μg/ml of poly-L-lysine (Sigma-Aldrich) and fixed with 0.5% glutaraldehyde (Sigma-Aldrich) in 24-well plates. The glasses were then incubated with 50 nM of CADM1-EC-Fc or control mouse IgG for 10 min and blocked with 1% bovine serum albumin (BSA, Sigma-Aldrich) in Hank's Balanced Salt Solution (HBSS) (Invitrogen). Then, MDCK cells (3×10^4) were plated on the glasses and incubated at 37°C for 60–70 min as indicated. After incubation, cells were fixed with 4% paraformaldehyde and subjected to immunofluorescence labeling with Alexa Fluor-labeled phalloidin. Cells were imaged with an epifluorescence microscope (Zeiss), and the surface area of GFP positive cells was measured by the AutoMeasure software module, AxioVision Version 4 (Zeiss). To evaluate the activities of inhibitors, the surface area of cells with each inhibitor was normalized to that of cells on IgG with DMSO, and then the value of cells on CADM1-EC-Fc with DMSO was set as 1. More than 100 cells were counted, at least, for each assay as indicated in the legend for each Figure as reported previously [15]. Statistical differences were determined by Student's t-test.

Immunofluorescence Microscopy

Cells were fixed with 4% paraformaldehyde for 20 min, quenched with 50 mM of NH_4Cl, and permeabilized with 0.1% Triton X-100 in PBS for 5 min. Cells were then blocked with 5% (w/v) fetal bovine serum in phosphate-buffered saline (PBS) and then incubated with primary and secondary antibodies sequentially with extensive washes between the incubation of different antibodies. Coverslips were then mounted with ProLong® Gold (Invitrogen), and cells were imaged with the epifluorescence microscope (Zeiss). Negative controls without primary antibodies were included in all experiments.

Glutathione S-transferase (GST) Pull-down Assay

The GST- or His-fusion protein was expressed in Rosetta DE3 *Escherichia coli* and isolated with glutathione Sepharose 4B (GE Healthcare) or Ni-NTA Agarose (QIAGEN), respectively, according to the manufacturers' protocols. For *in vitro* binding, the His-MPP3-N protein was incubated with GST-fusion proteins of CADM1 for 15 min at 4°C in a reaction buffer (50 mM of Tris-HCl, pH 7.4, 137 mM of NaCl, 0.1% Triton X-100, 10% glycerol, 0.5% BSA). The His-Dlg-N protein was added and incubated for 15 min, and then Glutathione Sepharose beads were added and further incubated for 1 h at 4°C. Beads were washed with reaction buffer and subjected to SDS-PAGE and Western blotting with anti-His antibodies. GST fusion proteins were detected by staining with Coomassie Brilliant Blue (CBB).

Results

Recombinant Extracellular Domain of CADM1 Mimics *Trans*-Homophilic Interaction of CADM1 and Induces Cell Spreading

We first established this cell spreading assay to identify the signaling pathway specifically activated by *trans*-homophilic interaction of CADM1 mediated by intercellular adhesion. MDCK cells stably expressing CADM1-GFP (MDCK+CADM1-GFP) or parental MDCK cells were incubated on the glass coated either with mouse IgG or with the recombinant CADM1-EC-Fc protein consisting of the extracellular fragment domain of CADM1 fused to the Fc region of mouse IgG. The following immunofluorescence staining of the actin cytoskeleton revealed that MDCK+CADM1-GFP cells showed large spread morphology when incubated on CADM1-EC-Fc-coated glass. By contrast, parental MDCK cells incubated on IgG- or CADM1-EC-Fc-coated glass or MDCK+CADM1-GFP cells incubated on IgG-coated glass showed round but not spread morphology (Fig. 1A and S1A). When the surface of the cells was measured quantitatively, the average surface area of MDCK+CADM1-GFP cells on CADM1-EC-Fc was 1.8-fold larger than that of the same cells on control IgG, although the size of the surface area was varied in each cell (Fig. 1B). To confirm that the spreading of the cells observed is mediated by *trans*-homophilic interaction of CADM1, the same assay was performed in the presence of the anti-CADM1 antibody, 9D2, which was shown to act as a blocking antibody [16]. As shown in Fig. S1B and 1B, the surface area of MDCK+CADM1-GFP cells incubated on CADM1-EC-Fc decreased significantlywhen incubated with the 9D2 antibody,

whereas the area was not changed with control IgY. Moreover, the surface area of MDCK+CADM1-GFP cells was not changed by 9D2 when incubated on IgG. These results suggest that cell spreading in this assay was specifically induced by the *trans*-homophilic interaction of CADM1. Since the actin cytoskeleton is one of the main determinants of cell shape, we then investigated the effect of Cytochalasin D, an inhibitor of actin polymerization, on CADM1-mediated cell spreading. As shown in Fig. S1C and 1C, spreading of MDCK+CADM1-GFP cells on CADM1-EC-Fc-coated glass was abrogated by Cytochalasin D, but not by control DMSO. These findings suggest that the *trans*-homophilic interaction of CADM1 induces cell spreading through reorganization of the actin cytoskeleton.

Next, we investigated whether the cytoplasmic domain of CADM1 is responsible for cell spreading. To examine this, MDCK cells were stably transfected with an expression vector of a truncated form of CADM1 lacking its cytoplasmic domain that was fused to YFP (ΔCT-YFP) and subjected to cell spreading assay (Fig. 1D). It should be noted that CADM1-ΔCT-YFP was localized at cell-cell contact sites similarly to full-length CADM1 tagged with YFP (FL-YFP) in confluent MDCK cells (Fig. S1D). The surface area of MDCK cells expressing CADM1-ΔCT-YFP is significantly smaller than that of CADM1-FL-YFP cells and not different from that of MDCK cells with CADM1-ΔCT-YFP incubated on control IgG (Fig. S1E and 1E). These findings suggest that the cytoplasmic domain of CADM1, and its cytoplasmic binding proteins as well, is essential for activating signaling for the actin reorganization to lead to cell spreading.

The PI3K Inhibitor Suppresses the Cell Spreading Mediated by *Trans*-homophilic Interaction of CADM1

The above findings prompted us to investigate the signaling pathway activated by CADM1-mediated cell adhesion to induce actin reorganization using cell spreading assay by treating cells with chemical compounds from the SCADS inhibitor kit (see Materials and Methods) and assessing the suppressor activity of each inhibitor in cell spreading. Among 104 chemicals we screened, two inhibitors of PI3K, LY294002 and Wortmannin, effectively suppressed cell spreading (Fig. S2A). The average cell areas treated with LY294002 and Wortmannin are 53% and 54%, respectively, in comparison with that treated with DMSO as 100%. On the other hand, the average cell surface areas treated with inhibitors of MAPK, JAK, and NF-KB in the same assay were 94%, 109%, and 96%, respectively, suggesting that the suppressor effect in cell spreading by PI3K inhibitors is significant. To confirm this inhibitory effect precisely, cells were then treated with different concentrations of LY294002, from 0.01 to 10 μM, and subjected to cell spreading assay. As shown in Fig. S2B and 2A, the surface area decreased by the treatment of LY294002 in a dose-dependent manner, where a significant difference was observed when it was treated with 1 and 10 μM of LY294002 as compared with DMSO. To exclude the possibility that LY294002 has a non-specific cytotoxic effect, cells were treated with 1 μM of LY294002 for 45 min and then washed and incubated with a fresh medium without LY294002 for an additional 45 min. Comparison of the surface area of cells revealed that cell spreading was suppressed in the presence of LY294002 for 90 min, while the suppressing effect was abrogated and the cell spreading was recovered when LY294002 was washed out (Fig. S2C and 2B), indicating that cell spreading was not irreversibly suppressed by the cytotoxicity of LY294002. Since the *trans*-homophilic interaction of CADM1 has been shown to induce cell aggregation in a suspension culture, we next examined the activity of LY294002 on CADM1-mediated cell aggregation. When cell aggregation assay was carried out, the degree of aggregate formation in cells treated with various concentrations of LY294002 did not show significant difference from that of DMSO-treated cells (Fig. 2C), showing that PI3K is not involved in intercellular adhesion activity by CADM1. These results suggest that CADM1-mediated *trans*-homophilic interaction activates PI3K to induce cell spreading but does not participate in cell aggregation activity.

Activation of the Pathways Downstream of PI3K, Akt, and Rac1 Is Necessary for CADM1-mediated Cell Spreading

Then, we analyzed how PI3K was activated by CADM1-mediated cell attachment to lead cell spreading. Since PIP_3 is a major product of PI3K signaling at the plasma membrane and specifically binds to the PH domain of Akt [17], PI3K activity can be detected by the exogenously expressed fluorescent Akt-PH in the cells. Here, to examine PI3K activation and its subcellular localization, MDCK cells expressing CADM1 without tags (MDCK+CADM1) were transiently transfected with a protein fragment of the PH domain of Akt tagged with GFP (GFP-Akt-PH) and subjected to spreading assay. After 45 min of incubation on a CADM1-EC-Fc-coated plate, strong signals of GFP-Akt-PH were detected at the leading edges of MDCK+CADM1 cells where actin-rich lamellipodia were generated, indicating that PI3K is activated at the leading edges of cells in CADM1-induced cell spreading (Fig. 3A).

We further examined the activation of Akt, a well-established downstream target of PI3K for actin remodeling, in CADM1-mediated cell spreading [18]. In Western blotting analysis, the increased intensity of the signal from phosphorylated Akt was detected in MDCK+CADM1-GFP cells cultured on the CADM1-EC-Fc-coated plate as compared with that of the cells on IgG, whereas no signal was detected when cells were treated with 10 μM of LY294002 (Fig. 3B). These results suggest that phosphorylation of Akt participates in CADM1-mediated cell spreading as a possible downstream effector of the PI3K pathway. However, when examined in the cell spreading assay, the inhibitor of Akt only partially suppressed spreading of MDCK+CADM1-GFP cells as compared with LY294002 when cultured on CADM1-EC-Fc, suggesting that some additional effectors would participate in the PI3K signaling (Fig. 3C). Then we examined Rac1, another effector of PI3K implicated in actin remodeling [19]. As shown in Fig. S2D and 3C, the Rac1 inhibitor only partially suppressed CADM1-mediated cell spreading as compared with LY294002 as the Akt-inhibitor did. However, when cells were treated with both Akt- and Rac1- inhibitors simultaneously, the surface area of MDCK+CADM1 cells decreased dramatically without any significant difference from those treated with LY294002, indicating that the Akt- and Rac1- inhibitors worked additively to suppress cell spreading. These findings indicate that both Akt and Rac1 are key effectors of PI3K when activated by CADM1-mediated cell spreading.

CADM1 Forms a Multi-protein Complex with MPP3, Dlg, and PI3K

Finally, we analyzed possible molecules that connect CADM1 with PI3K leading to cell spreading. It has been reported that the regulatory subunit of PI3K, p85, interacts with one MAGuK, Dlg, and is recruited to cell-cell contact sites in epithelial cells [20]. Dlg further binds to another MAGuK, MPP3, which was identified as a binding partner of the cytoplasmic domain of CADM1 through their N-terminal domain [8,21], suggesting that MPP3 and Dlg are candidates for connecting CADM1 with PI3K. To examine

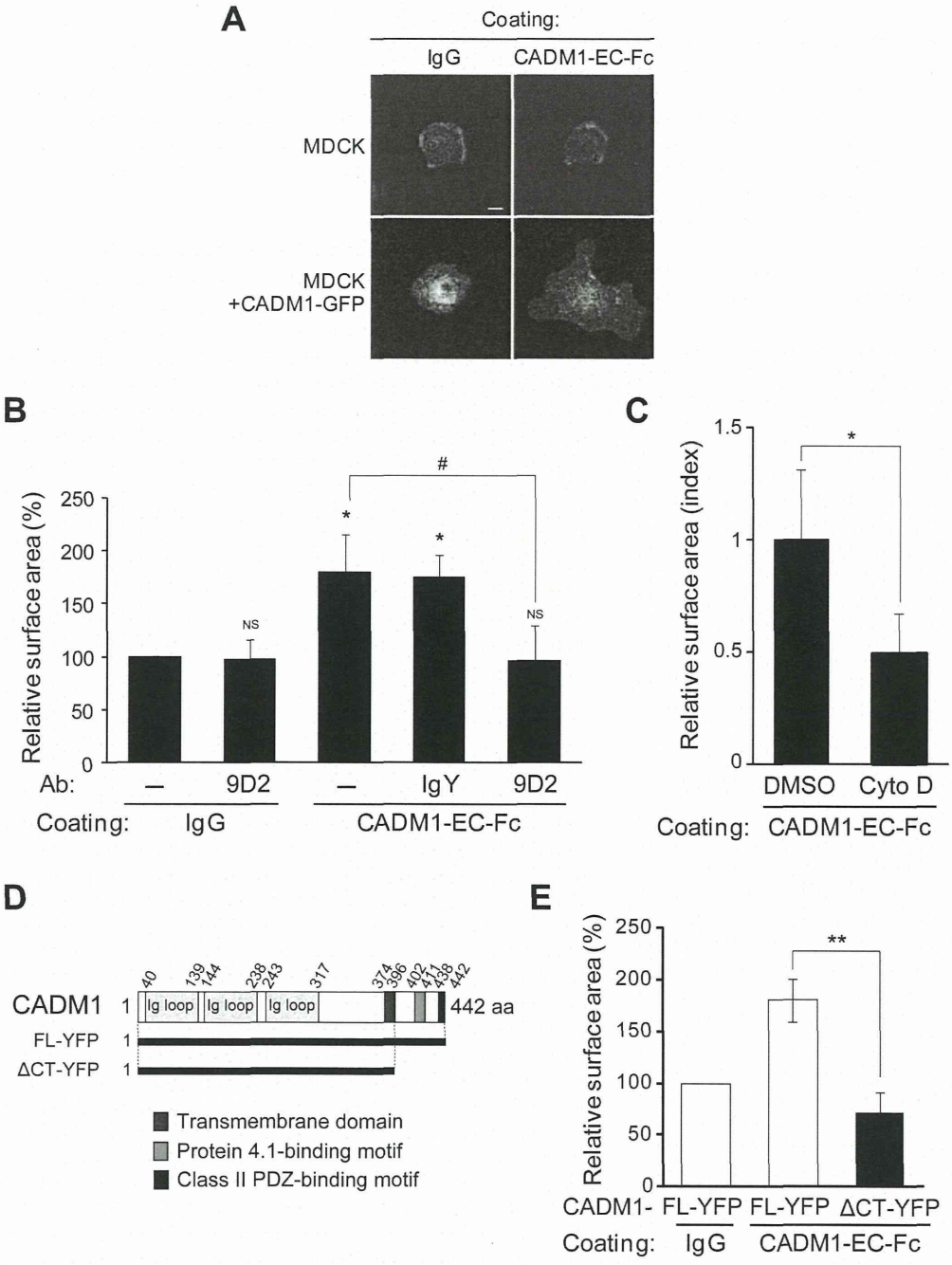

Figure 1. Recombinant extracellular domain of CADM1 mimics the *trans*-homophilic interaction of CADM1 and induces cell spreading. Parental MDCK cells or MDCK cells stably expressing CADM1-GFP (MDCK+CADM1-GFP) were incubated on coverslips coated with control IgG or recombinant proteins consisting of the extracellular fragment of CADM1 fused to Fc fragments of mouse IgG (CADM1-EC-Fc). After 60 min, the cells were visualized by staining the actin cytoskeleton with Alexa Fluor 568-labeled phalloidin. (A) Representative images of F-actin in cells incubated on control IgG- or CADM1-EC-Fc-coated glasses as indicated. Bars: 20 μm. (B) MDCK+CADM1-GFP cells were incubated on IgG or CADM1-EC-Fc in the presence or absence of control human IgG or anti-CADM1 antibody, 9D2 (10 μg/ml). Cell spreading was quantified by measuring the average surface area of cells. Relative value to cells on the IgG-coated glass without antibodies was shown. More than 100 cells were counted in the assay. *, $p<0.05$; NS, no significant difference (vs. cells on IgG without antibodies). #, $p<0.05$. (C) Cell spreading assay using MDCK+CADM1-GFP cells incubated on IgG or CADM1-EC-Fc with DMSO or 1 μM of Cytochalasin D (Cyto D). The area was normalized to that of cells on IgG with DMSO, and the relative value to cells on CADM1-EC-Fc with DMSO was shown. More than 180 cells were counted in the assay. *, $p<0.05$. (D) A schematic representation of CADM1 protein structure. The YFP-fusion proteins of full-length CADM1 (CADM1-FL) and its deletion mutant lacking the cytoplasmic fragment (CADM1-ΔCT) were shown. (E) Cell spreading assay of MDCK cells stably expressing CADM1-YFP-FL or CADM1-YFP-ΔCT that were incubated on IgG or CADM1-EC-Fc. Relative value of cell surface area to that of CADM1-YFP-FL cells on IgG-coated glass was shown. More than 230 cells were counted in the assay. **; $p<0.01$. (B, C, and E) The results presented are mean ± SD of three independent experiments.
doi:10.1371/journal.pone.0082894.g001